Reprinted from Preprint Volume: 12th Conference on Severe Local Storms, Jan. 11-15, 1982; San Antonio, Tex. Published by the American Meteorological Society, Boston, Mass.

THE LIFE CYCLE OF THUNDERSTORM GUST FRONTS AS VIEWED WITH DOPPLER RADAR AND RAWINSONDE DATA

Roger M. Wakimoto
The University of Chicago
Chicago, Illinois

1. INTRODUCTION

The gust front originating from a mature thunderstorm is a commonly observed phenomenon. In recent years there has been increased interest to understand its structure and mechanism. Quantitative data on the low-level structure of the gust front as it passes a 500-m instrumented tower have been presented by Charba (1974) and Goff (1976). These studies assume that the gust front is a steady state phenomenon in order to use a time-space conversion (Fujita,1963) to construct a two dimensional analysis. Laboratory tank models of density currents have been developed (Middleton, 1966; Simpson, 1969, 1972) to deduce the gust front structure above the instrumented tower heights. Although these lab experiments have been very useful, they have been unable to prove unequivocably that the dynamics of the gust front are the same as the density current. As an extension of these past studies, three main objectives of this paper are:

1. to depict the entire vertical structure of the gust front,
2. to obtain the time-dependent analysis of the gust front,
3. to investigate the dynamics of the gust front.

2. THE THUNDERSTORM GUST FRONT

The case studies analyzed from Project NIMROD (Figure 1) are gust fronts from squall lines many tens of kilometers in length. As a result of these analyses, four stages of the life cycle of the gust front came to light. These stages are presented in Figure 2. Examples from the gust front of 17 June 1978 (Case C) are shown to illustrate three of the four stages. For a thorough discussion of all four stages of the thunderstorm gust front, refer to Wakimoto (1981).

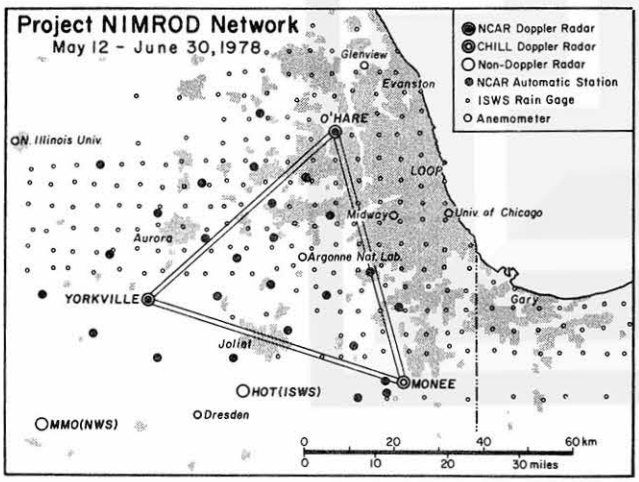

Figure 1. The NIMROD network.

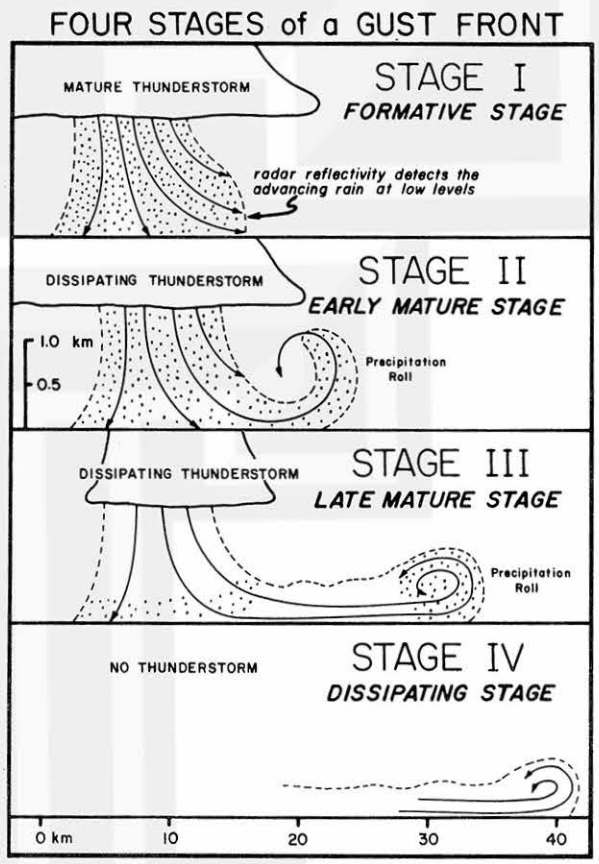

Figure 2. The four stages of a thunderstorm gust front. The advancing precipitation a low levels is detected by the radar. The "precipitation roll" is a horizontal roll formed by precipitation which is forced ahead of the squall line by the downdraft.

In Figures 3 and 4, a complete time history of the development of the gust front of Case C is shown. Four times were chosen to construct vertical cross sections: 2221 (stage I),2224 (stage II), 2227 (stage III), and 2233 (stage III) CDT.

At 2221 CDT (stage I), a rain band is approaching the surface,indicated by the 40 dBZ echo core (Figure 4). Some of this precipitation is flowing horizontally away from the squall line at a Doppler speed of 22 m/s. The reflectivity contours for the heights less than 1.2 km are slightly ahead of the squall line, as shown in the model of stage I in Figure 2. This is a result of the downdraft striking the ground and being forced horizontally

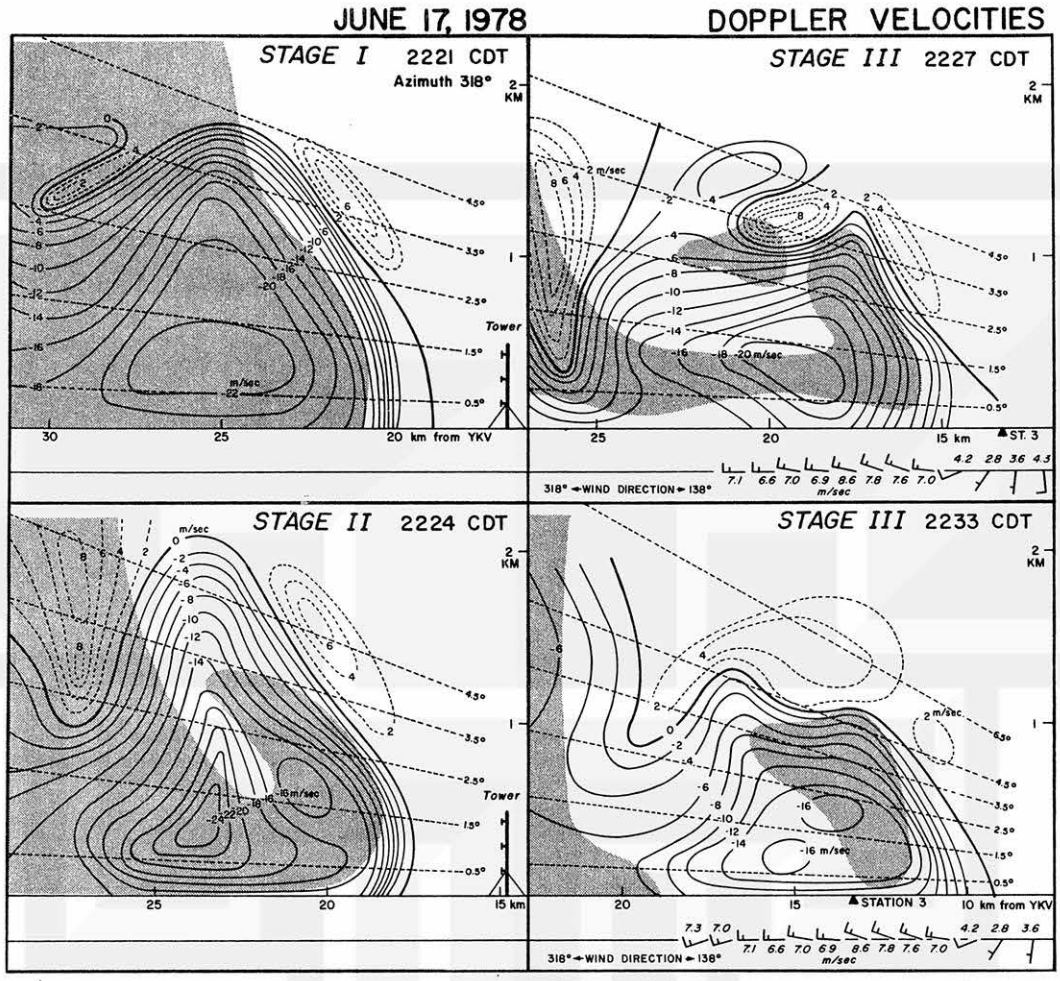

Figure 3. RHI cross sections of Case C at 2221 (stage I), 2224 (stage II), 2227 (stage III), and 2233 (stage III) CDT. Dashed lines are Doppler velocities away from the radar and solid lines are velocities toward the radar. The gray shade is the areas of 10 dBZ reflectivity or greater (see Figure 4). Distances are measured from YKV along the 318° azimuth. Surface data is obtained from PAM station 3. Located in the lower right hand corner of the 2221 and 2224 CDT analyses is a 500-m tower to represent the maximum height of past studies on the gust front.

toward the leading edge of the outflow. Past radar studies have overlooked this feature since it occurs on a very small scale.

Charba (1974) envisioned the streamline pattern of the formation stage of a gust front to be similar to a vertical jet of fluid striking a plane surface. As shown in Figure 4 (2224 CDT), Charba has described an excellent analogy of the flow as there is an upward push of precipitation approximately 20 km from the radar. The flow is well correlated with the reflectivity pattern as the strongest vertical velocities are confined to the leading edge of the precipitation. This is the beginning of the precipitation roll. The roll is a new finding defined as follows,

> precipitation roll: a reflectivity pattern of precipitation shown by the Doppler velocities to be revolving in a horizontal roll at the gust front.

By 2227 CDT (stage III), the precipitation has pushed well ahead of the squall line, but still appears to have a physical connection with the source. The 15 dBZ isoline located 22 km from the radar is a core of precipitation propagating toward the head of the gust front. It is during stage III that the gust front characteristics are the same as a density current.

The precipitation roll becomes completely disjointed from the squall line at 2233 CDT (stage III), as shown by the Doppler velocity pattern (Figure 3). Note how the relative motion vectors conform to the reflectivity echoes in Figure 4. The relative circulation center is near the center of the 15 dBZ isoline located in the head.

3. DYNAMICS OF THE GUST FRONT

3.1 Nonhydrostatic versus hydrostatic pressure

Surface weather observations are combined with serial rawinsonde ascents at Yorkville IL to determine the nature of the pressure rise associated with the passage of a gust front. Of particular interest is the rise in pressure before the arrival of the cold air.

Calculations of the increase in hydrostatic pressure based on the average temperature before and after the passage of the gust front are

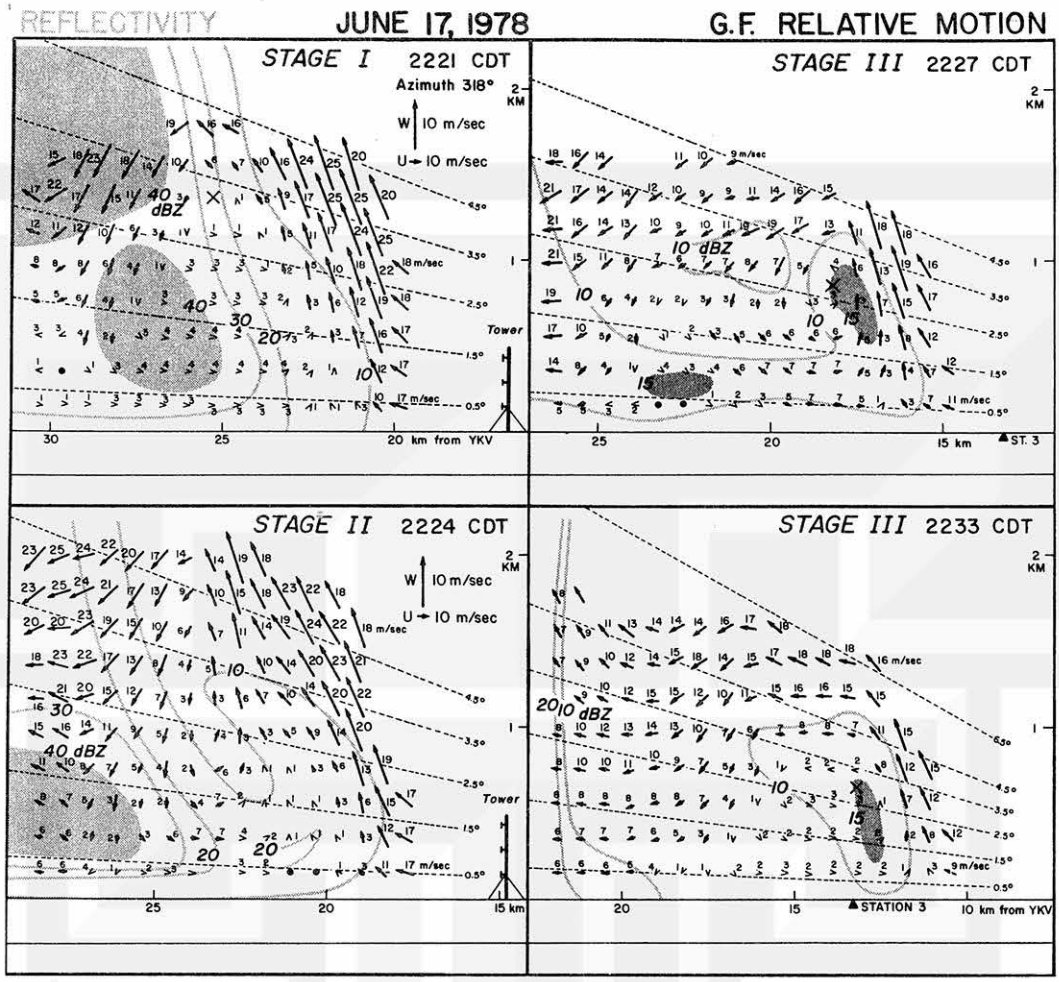

Figure 4. RHI cross sections of the gust front-relative motion for Case C at 2221 (stage I), 2224 (stage II), 2227 (stage III), 2233 (stage III) CDT. The "X" denotes the relative circulation center. Light gray areas are reflectivities greater than 40 dBZ. Dark gray areas are reflectivities greater than 15 dBZ but less than 20 dBZ.

shown in Table 1. The observed versus calculated hydrostatic pressure rise agree amazingly well.

A persistent question that appears in much of the literature is the rise in pressure before the arrival of the gust front. There have been instances when this pressure rise could be a pressure jump (Tepper, 1950; Fujita, 1963; Charba, 1974), but this phenomenon is not sufficient to explain all of the cases. The nonhydrostatic pressure at the frontal interface appears to be the major contributor to the observed pressure rise.

If the ambient air is stagnant, Newton (1963) stated that a nonhydrostatic pressure was produced by a cold air outflow. The magnitude would be governed by,

$$P_{nh} = \frac{1}{2}\rho V^2 \qquad (1)$$

P_{nh} = the nonhydrostatic pressure
ρ = the density of the cold air
V = the windspeed in the cold air.

expanding Newton's idea to a situation when the ambient is not stagnant would lead to values of a nonhydrostatic pressure in the warm air. These calculations are summarized in Table 2.

There appears little doubt that the pressure rise in advance of the gust fronts observed during NIMROD were caused by the collision of two fluids of different densities.

Table 1
Calculations on the hydrostatic pressure rise behind the gust front. $\overline{T}_w$ and $\overline{T}_c$ is the mean temperature in the warm and cold air.

	Case A	Case B	Case C
$\overline{T}_w$ (°C)	16.19	19.20	24.76
$\overline{T}_c$ (°C)	13.00	16.15	20.76
cold air depth (m)	3953	2236	1340
observed pressure rise (mb)	5.2	1.6	1.2
calculated pressure (mb)	4.5	1.8	1.3

To examine the effect of the gradient of nonhydrostatic pressure on the environmental winds, a simplified model will be derived. It is assumed that the flow is frictionless, irrotational, homogeneous, and is confined to the x-z plane perpendicular to the gust front. The equation of motion in the x-direction reduces to,

$$\frac{\partial u}{\partial t} + u\frac{\partial u}{\partial x} = -\frac{1}{\rho}\frac{\partial p}{\partial x} = \text{const.} = C \qquad (2)$$

Using the time-space conversion, a derivative in space can be converted into a deriva-

Table 2
Nonhydrostatic pressure calculations

	Case A	Case B	Case C
calculated nonhydrostatic pressure (mb)	2.34	0.48	0.65
observed nonhydrostatic pressure (mb)	2.50	0.50	0.65

tive in time. Thus Eq. (2) becomes

$$\frac{\partial u}{\partial t} + \frac{u}{V}\frac{\partial u}{\partial t} = C \qquad (3)$$

V = propagation speed of the gust front.

Eq. (3) can be rewritten as

$$(u^2 + 2Vu)_t = 2VC\Delta t \qquad (4)$$

where the equation has been integrated from $t = 0$ to $t = t$, and u is assumed to be zero at the initial time.

Eq. (4) is a simple quadratic in u and can be easily solved. The results are shown in Table 3. There is good agreement between observed and calculated decreases of windspeed in the warm air despite the simplicity of the model. Apparently, the gradient of the nonhydrostatic pressure in the direction perpendicular to the frontal interface is responsible for the decrease in the normal component of the windspeed to a minimum before the arrival of the cold air. This windspeed minimum may be regarded as "the calm before the storm" described by numerous observers.

Table 3
The effect of the gradient of nonhydrostatic pressure on the windspeed in the warm air.

	Case A	Case B
calculated decrease in windspeed (m/s)	8.7	3.6
observed decrease in windspeed (m/s)	10.0	5.3

Based on the surface observations from NIMROD, a model of the gust fronts in stages II and III is presented in Figure 5.

3.2 Propagation Speed of the Gust Front

The equation for the speed of the leading edge of a density current was applied to the gust front observed during NIMROD to establish if they were dynamically similar. This equation is expressed as,

$$V = k\left(gd\,\frac{\bar{\rho}_c - \bar{\rho}_w}{\bar{\rho}_w}\right)^{\frac{1}{2}} \qquad (5)$$

Using rawinsonde data, mean densities in the warm and cold air were calculated. By substituting the observed propagation speed into Eq. (5), values of k could be compared with those found in the literature. In Table 4, a mean value of k was calculated to be 0.77. Most researchers agree that the k -value for a density current is 0.75.

From the results of Tables 3 and 4, it is concluded that the predominate driving force for the gust front is the horizontal pressure gradient

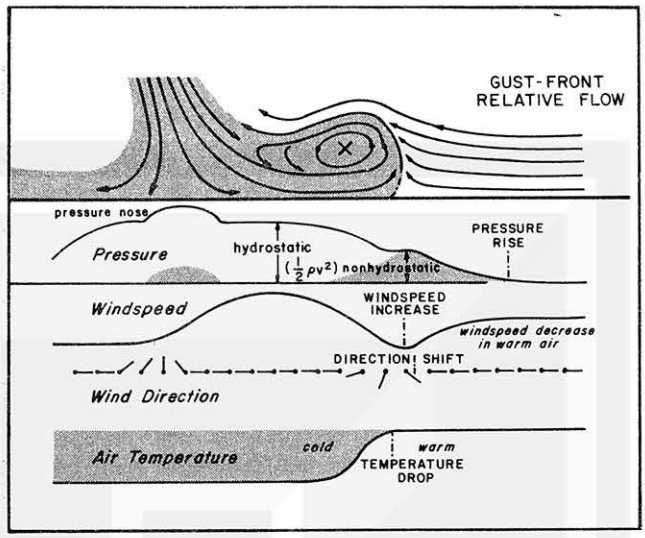

Figure 5. Conceptual model of the surface observations during the passage of a gust front in stages II and III.

Table 4
Propagation speed of the gust front.

		Case A	Case B	Case C
$\bar{\rho}_c$	cold air (10^{-4} g/cm^3)	9.66	10.41	10.87
$\bar{\rho}_w$	warm air (10^{-4} g/cm^3)	9.55	10.39	10.69
d	depth (m)	3954	2235	1332
V	propagation speed (m/s)	20	7	13
k	Froude number	0.76	0.71	0.87

$\bar{k} = 0.77$

acting across the interface caused by the greater hydrostatic pressure in the cold air (i.e. a density current). It is interesting to note that the vertical transfer of momentum provided by the downdraft does not play a role in determining the propagation speed. Of course, in the early stages (I or II), Eq. (5) could not be expected to accurately predict the motion of the outflow.

Acknowledgement:- Research supported by NOAA, Grant No. NA80OAA-D-00001; NASA, Grant No. NGR 14-001-008; and NSF, Grant No. ATM 79-21260.

REFERENCES

Charba, J., 1974: Applications of the gravity current model to analysis of squall-line gust fronts, Mon. Wea. Rev., 102, 140-156.

Fujita, T.T., 1963: Analytical mesometeorology: A review, Meteorological Monographs (Severe Local Storms), Vol 5, No. 27, 77-125.

Goff, R.C., 1976: Vertical structure of thunderstorm outflows, Mon. Wea. Rev., 104, 1429-1440.

Middleton, G.V., 1966: Experiments on density and turbidity currents, Part I: Motion of the head, Can. J. Earth Sci., 3, 523-546.

Newton, C.W., 1963: Dynamics of severe convective storms, Meteorological Monographs, (Severe Local Storms), Vol 5, No. 27, 33-55.

Simpson, J.E., 1969: A comparison between laboratory and atmospheric density currents, Quart. J. Roy. Meteor. Soc., 95, 758-765.

Simpson, J.E., 1972: Effects of the lower boundary on the head of a gravity current, J. Fluid Mech., 53, pt 4, 759-768.

Tepper, M., 1950: A proposed mechanism of squall lines: the pressure jump line, J. Meteor., 7,, 21-29.

Wakimoto, R.M., 1981: Investigations of thunderstorm gust fronts using Project NIMROD data, Ph. D. thesis, Dept. of Geophysical Sciences, Univ. of Chicago, 129 pp.